Analytica Chimica Acta 1195 (2022) 339386

Contents lists available at ScienceDirect

Analytica Chimica Acta

journal homepage: www.elsevier.com/locate/aca

Chemiluminescence sensing of adenosine using DNA cross-linked hydrogel-capped magnetic mesoporous silica nanoparticles

Yanan Hou , Rui Han , Yuanling Sun , Chuannan Luo *, Xueying Wang **

Key Laboratory of Interfacial Reaction & Sensing Analysis in Universities of Shandong, School of Chemistry and Chemical Engineering, University of Jinan, Jinan, 250022, PR China

HIGHLIGHTS

- The loading rate of DNA cross-linked hydrogel-capped mesoporous silica nanoparticles was effectively increased.
- MIL-101 (Fe), as a signal amplified material, improved the detection sensitivity.
- The aptamer DNA chain acts as a "switch" to prevent luminol from leaking.
- The CL biosensor was successfully used for adenosine determination in actual samples.

GRAPHICAL ABSTRACT

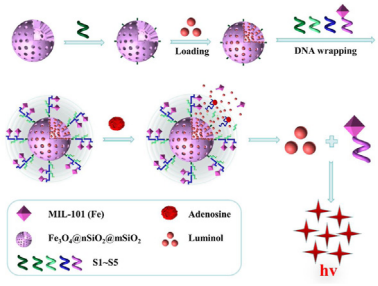

ARTICLE INFO

Article history:
Received 16 September 2021
Received in revised form
9 December 2021
Accepted 17 December 2021
Available online 7 January 2022

Keywords:
Chemiluminescence
Adenosine
Metal organic framework
Magnetic mesoporous silica nanoparticles
DNA hydrogels

ABSTRACT

At present, a host of high-sensitivity and selective tumor marker detection methods play a central role in various research fields and assay platforms. Here, a method for DNA cross-linked hydrogel-capped magnetic core-shell structure mesoporous silica nanoparticles (Fe_3O_4@nSiO_2@mSiO_2) based on target stimulus was proposed. Specifically, Fe_3O_4@nSiO_2@mSiO_2 nanoparticles with nucleic acid promoter units were prepared. The promoter induces the predesigned modified polyacrylamide DNA strand to carry out hybridization chain reaction on the surface of Fe_3O_4@nSiO_2@mSiO_2 nanoparticles, forming a hydrogel coating on the surface of Fe_3O_4@nSiO_2@mSiO_2 nanoparticles. Under the stimulation of adenosine, Fe_3O_4@nSiO_2@mSiO_2 released the signal molecule luminol. Simultaneously, the MIL-101 (Fe) material, a signal amplification molecule, was released from the DNA hydrogel. Compared with the traditional gated mesoporous silica system, the DNA hydrogel-coated Fe_3O_4@nSiO_2@mSiO_2 is not easy to leak and has a higher loading capacity. In addition, the optical background of DNA hydrogels is low, combined with MOFs materials, even about 1.4×10^{-10} M adenosine can be detected in this biosensor. Based on the combination of DNA hydrogels, MOFs conjugates and gating systems, the construction of biosensors will be more eye-catching, which will expand new ideas for biosensor platform manufacturing.

* Corresponding author. Key Laboratory of Interfacial Reaction & Sensing Analysis in Universities of Shandong, School of Chemistry and Chemical Engineering, University of Jinan, Jinan, 250022, PR China.
** Corresponding author.Key Laboratory of Interfacial Reaction & Sensing Analysis in Universities of Shandong, School of Chemistry and Chemical Engineering, University of Jinan, Jinan, 250022, PR China.
E-mail addresses: chm_yfl518@163.com (C. Luo), chm_wangxy@ujn.edu.cn (X. Wang).

https://doi.org/10.1016/j.aca.2021.339386
0003-2670/

1. Introduction

Adenosine is an endogenous regulator of neuronal excitability and has anticonvulsant and neuroprotective effects. In addition, adenosine overexpression is often associated with tumorigenesis [1]. Fast-growing solid tumors can cause local hypoxia in the tissues and accumulate large amounts of adenosine [2]. Therefore, the detection of adenosine content is of great significance for the practical clinical diagnosis of solid tumors. Biosensors are basic tools for analyzing biomarkers variations in vivo. Recently, people have made tremendous efforts to build varieties of promising biosensor platforms (including fiber optic particle plasmon resonance biosensor [3], photoelectrochemical biosensor [4], optical biosensor [5], fluorescent biosensor [6–8], microbial fuel cells (MFCs) biosensor [9], electrochemical biosensor [10], colorimetric biosensor [11–14] to effectively detect biomarkers. With its unique advantages of low background noise, high sensitivity and simple instrument [15], chemiluminescence has stimulated researchers' strong interest in biosensor design, and its applications range from environmental analysis to clinical diagnosis and related fields. The most classic chemiluminescence reaction is that luminol is oxidized by hydrogen peroxide in alkaline medium [16,17]. He et al. prepared AuNPs/MOGs (Fe) using an in-situ growth method and discovered a new chemiluminescence method for detecting organophosphorus pesticides [18]. Lu et al. constructed a chemiluminescence sensor based on FeCo alloy@N-doped carbon layers with peroxidase-like activity, and the sensor successfully detected glucose [19]. Based on this, it is necessary to find some methods to expand the application of chemiluminescence. But bioensors that combine the advantages of chemiluminescence and controlled release systems are rare [20–22].

The latest report about mesoporous silica and its derivatives has been widely used in controlled release systems. The system can be triggered by different stimuli, such as temperature, pH, magnetic field, etc [23–27]. Recently, a controlled release system based on mesoporous silica nanoparticles has been combined with a variety of detection technologies to establish biosensors for detecting different targets. Mar Oroval et al. used MCM-41 to load rhodamine B, and the aptamer chain blocked the mesopores of MCM-41 through electrostatic interaction. Based on this, the constructed controlled release system successfully detects As(III) [28]. Gu et al. used DNA nuclease or bacterial lysate to decompose the DNA gate, the mesoporous silica released hemin to catalyze the chemiluminescence system, and finally successfully detected *Escherichia coli O157:H7* (*E. coli*) or *Staphylococcus aureus* (*S. aureus*) [29]. Mesoporous silica is a strong candidate for the development of low-cost chemiluminescent biosensors. However, the participation of mesoporous silica in the traditional mesoporous silica controlled release system will affect the background signal, so the intervention of magnetic materials is necessary. In addition, the risk of leaking the loaded material after the pore size is closed, compared with the traditional controlled release technology, the controlled release system that uses DNA hydrogels to block the mesoporous silica has advantages. DNA hydrogel is a three-dimensional network formed by Watson-Crick base pairing. DNA hydrogel has biocompatibility, adjustable mechanical and chemical properties, and exhibits a sensitive response to external stimuli [30]. These unique properties make DNA hydrogels have great potential in applications such as biosensors, environmental analysis, and controlled drug release [31–33].

Classically, the chemiluminescence reaction based on luminol is widely used for its low price and high sensitivity. But the original chemiluminescence signal is very weak. Therefore, various nanozymes are widely used to amplify signals, such as metal-organic framework [34–36] and DNA nanotechnology [37–40]. As a well-known metal-organic framework, the iron-based metal-organic framework has the ability to combine with polymers, proteins, ions and aptamers [41]. Many biosensors based on iron-based metal organic frameworks have been studied, which can detect proteins, nucleic acids, viruses, and cancer cells with high sensitivity and selectivity [42,43]. He et al. used the electrostatic interaction between MIL-101 and aptamers to construct a fluorescent amplification strategy biosensor for sensitive detection of thrombin and oxytetracycline [44]. Luan et al. used DNAzyme-labeled Fe-MIL-88-Pt combined with circular strand-displacement polymerization to amplify the signal of the colorimetric biosensor platform. Finally, the platform successfully detected chloramphenicol [45].

In this work, a chemiluminescence biosensor based on cross-linked hydrogel-capped magnetic core-shell structure mesoporous silica (Fe_3O_4@nSiO_2@mSiO_2) nanoparticles was designed. First, the surface of the synthetic Fe_3O_4@nSiO_2@mSiO_2 was modified by surface amination, and then the mesopores of Fe_3O_4@nSiO_2@mSiO_2 were used to load a large amount of luminol. Finally, the modified polyacrylamide DNA strands were cross-linked to form the DNA hydrogel shell. The DNA hydrogel can retain the skeleton structure of the hydrogel and make the DNA hydrogel biocompatible. In addition, mil-101 (Fe), which as a peroxidase-like, was incorporated into DNA hydrogels to amplify chemiluminescence signals. Adenosine binds to the aptamer through strong specific recognition, which acts as a switch to open the gate of the mesoporous silica, and then luminol as the signal molecule was released. Magnetic mesoporous silica can effectively avoid signal interference from loaded materials. This effective controlled release system provides a potential method for the detection of adenosine.

2. Experimental

2.1. Reagents and instruments

The detail was shown in Supporting Information. The DNA base sequences are as follow: DNA1 (S1), 3′-GGCTTTCGAAGAA-CA–$(CH_2)_6$–NH_2-5'; DNA2 (S2), 3′-TTGGAAGGAGGCGTTAT-GAGGGGGTCCAAGAGATATACCGAAAGCTTCTTG-5'; DNA3 (S3), 3′-AACGCCTCCTTCCAA-Acrydite-5'; DNA4 (S4), 3′-TATATCTCTTG-GACCCAATTCATGCATGACTAAGGGTTTAACTTGCTTGCCCTAGGT-Acrydite-5'; DNA5 (S5), 3′-TACGTACTGATTCCCTTT–$(CH_2)_6$–NH_2-5'. These sequences were purchased from Sangon Biotech Company (Shanghai, China).

2.2. Adenosine detection process

The prepared Fe_3O_4@nSiO_2@mSiO_2 was blocked by DNA hydrogel for quantitative analysis of adenosine, the experimental steps were as follows.

Step 1: Adenosine were added to the prepared DNA hydrogel-capped Fe_3O_4@nSiO_2@mSiO_2 and incubated for 60 min. The supernatant was obtained.

Step 2: Sample and NaOH flow through the main pump, Tris-buffer and H_2O_2 flow through the vice pump. The flow injection chemiluminescence analyzer was started to run for 311s to obtain CL intensity (I), as shown in Fig. S1.

2.3. Synthesis of Fe_3O_4@nSiO_2@mSiO_2-S1 and MIL-101(Fe)–S5

The preparation of Fe_3O_4@nSiO_2@mSiO_2 refers to the work that has been reported. Method for preparing Fe_3O_4 was shown in Supporting Information. At room temperature, 0.2 g Fe_3O_4 was dispersed in 200 mL 0.1 M HCl and ultrasonically dispersed for 10 min. After magnetic separation, Fe_3O_4 was washed three times

with H_2O, and then was dispersed in the mixed solution containing 160 mL ethanol, 40 mL H_2O and 2 mL NH_4OH. 0.2 mL Ethylsilicate (TEOS) was added dropwise to the vigorously stirred mixed solution and reacted for 6 h Fe_3O_4@nSiO_2 was washed with ethanol and H_2O respectively. Fe_3O_4@nSiO_2 was ultrasonically dispersed in the mixed solution containing 0.6 g cetyltrimethylammonium bromide (CTAB), 160 mL H_2O, 120 mL ethanol and 2.2 mL NH_4OH for 30 min. Then, the mixed solution was mechanically stirred. Then 0.6 mL TEOS and 0.4 mL 3-aminopropyltriethoxysilane (APTES) were added dropwise to it. After stirring for 6 h, the product was washed with ethanol and H_2O. Finally, in order to remove the porogen CTAB in Fe_3O_4@nSiO_2@mSiO_2, the mixture of Fe_3O_4@nSiO_2@mSiO_2 and 6 g/L ammonium nitrate-ethanol was transferred to a reactor with Teflon liner and reacted at 110 °C for 48 h. The product was washed with H_2O to obtain Fe_3O_4@nSiO_2@mSiO_2 with mesoporous structure [46].

After 5 mg Fe_3O_4@nSiO_2@mSiO_2 was activated by 0.1 mL glutaraldehyde for 2 h, 5 μL 3×10^{-6} M S1 was added it to incubate overnight. The product was washed with Tris-HCl buffer and magnetically separated. Fe_3O_4@nSiO_2@mSiO_2-S1 was stored at 4 °C.

The preparation method of MIL-101(Fe) refers to previously published work [47]. 0.6622 g $FeCl_3 \cdot 6H_2O$ and 0.2246 g 2-aminoterephthalic acid were dissolved in 15 mL DMF. Ultrasonic treatment for 15 min to completely dissolve the solid, the mixed solution was transferred to a reactor with Teflon liner and reacted for 20 h at 110 °C. The dark orange solid was obtained by centrifugation, which was purified twice with hot ethanol (60 °C, 3 h). Then, the purified product was dried at 70 °C for 30 min. Finally, the material was activated in an oven at 150 °C for 8 h.

0.5 mL glutaraldehyde was added into 100 mg MIL-101(Fe) to activate its amino group for 2 h, then 0.1 mL 2×10^{-4} M S5 was added the mixture and incubated for 8 h. After incubation, the mixture was centrifuge and the product was washed with Tris-HCl buffer. The product was stored at 4 °C.

2.4. Synthesis of DNA hydrogel-capped Fe_3O_4@nSiO_2@mSiO_2

4% acrylamide was added to the mixture containing 2.5 μL 0.1 mg/μL Fe_3O_4@nSiO_2@mSiO_2-S1, 5 μL 10^{-5} M S2, 5 μL 1.2×10^{-5} M S3, 12 μL 4.0×10^{-6} M S4 and 12 μL 0.2 g/L MIL-101(Fe)—S5, and deoxygenated at 37 °C for 10 min. The mixture was added with APS (0.15%) and TEMED (0.125%) to initiate polymerization. The polymer solution was incubated at 80 °C for 5 min, then incubated in an ice bath for 30 min to ensure effective closure between DNA. The residual monomer was removed by centrifugation.

3. Results and discussion

3.1. Experimental principles

In this work, a chemiluminescence biosensor based on cross-linked hydrogel-capped Fe_3O_4@nSiO_2@mSiO_2 nanoparticles was constructed. Firstly, the surface of the Fe_3O_4@nSiO_2@mSiO_2 was modified by amination, then the mesopores of Fe_3O_4@nSiO_2@mSiO_2 were used to load a large amount of luminol as the signal molecule. Finally, the modified polyacrylamide DNA chains were cross-linked to form DNA hydrogel. DNA hydrogel serves as a shell to retain the backbone structure of the hydrogel and make the DNA hydrogel biocompatible. In addition, as a peroxidase-like MIL-101(Fe) was also integrated into the DNA hydrogel to amplify the chemiluminescence signal. The controlled release system was completed by adenosine stimulating the release of luminol from Fe_3O_4@nSiO_2@mSiO_2 by opening the DNA hydrogel shell. The experimental schematic diagram is shown in Fig. 1.

3.2. Characterizations of Fe_3O_4@nSiO_2@mSiO_2

In Fig. 2(A-E), Fe_3O_4@nSiO_2@mSiO_2 has the core-shell structure with a uniform size of about 800 nm. The TEM image and SEM image of Fe_3O_4@nSiO_2@mSiO_2 with multiple images clearly shows that the thickness of the silicon dioxide layer of Fe_3O_4@nSiO_2 was about 10 nm, and the thickness of the mSiO_2 shell of Fe_3O_4@nSiO_2@mSiO_2 prepared after acetone removal of the CTAB template was about 50 nm. As shown in Fig. 2(F), in contrast to the smooth spherical shape of Fe_3O_4@nSiO_2@mSiO_2, the introduction of Mil-101(Fe) causes the sphere to appear as an octahedral tip, which is attributed to the successful attachment of Mil-101(Fe) to Fe_3O_4@nSiO_2@mSiO_2 and indicates the successful synthesis of Fe_3O_4@nSiO_2@mSiO_2-MIL-101(Fe). The additional TEM image (Fig. S2) and EDS spectrum (Fig. S3) further confirmed the successful preparation of Fe_3O_4@nSiO_2@mSiO_2-MIL-101(Fe).

In Fig. 3(A), the XRD image further was shown that the crystal form of the prepared Fe_3O_4@nSiO_2@mSiO_2 is perfect. The FTIR spectrum of Fe_3O_4@nSiO_2@mSiO_2 was shown in Fig. 3(B). 588 cm^{-1} is the characteristic vibration peak of Fe—O, and 1076 cm^{-1} is the stretching vibration peak of the partial Si—O—Si group. 1647 cm^{-1} is the bending vibration peak of $-NH_2$, and 2844 cm^{-1} and 2923 cm^{-1} are the stretching vibration absorption peaks of carbon-hydrogen bond. The removal of CTAB in the material leads to a decrease in the intensity of the absorption peak of C—H bond. 3447 cm^{-1} is the bending vibration peak of O—H. The FTIR spectroscopy showed that Fe_3O_4@nSiO_2@mSiO_2 was successfully prepared. According to the BET characterization in Fig. 3(C), Fe_3O_4@nSiO_2@mSiO_2 is a mesoporous nanomaterial with a pore diameter of about 3.5 nm and a specific surface area of 234.89 m^2/g. As shown in the UV spectrum (Fig. S4), the peak value of luminol after wrapping is significantly reduced compared with that before wrapping, which indicates that luminol was well encapsulated in the pore cavity of Fe_3O_4@nSiO_2@mSiO_2 through oligonucleotide chains (S1—S5).

3.3. Characterizations of MIL-101(Fe)

The SEM image of Fig. 3(D) shown that MIL-101(Fe) has a uniform octahedron, which is consistent with the work reported in previous reports. In the FTIR spectrum of MIL-101(Fe), the characteristic peak of O—H appears at 3462 cm^{-1}. The peak at 3379 cm^{-1} is the stretching peak of N—H. The strong peak at 1592 cm^{-1} is attributed to the stretching peak of O—C—O. The peak at 533 cm^{-1} corresponds to the characteristic peak of Fe—O. In Fig. 3(F), the diffraction peaks at $2\theta = 5.6°$, 5.8°, 8.4°, 9.0°, 10.3° and 16.5° correspond to (440), (531), (822), (911), (1022) and (1571) crystal planes of MIL-101(Fe) (CCDC 665510). The BET characterization of MIL-101(Fe) (Fig. S5) shows the specific surface area of MIL-101(Fe) is 28.25 m^2/g, and average pore diameter is 24.9 nm. The above proves that the synthesis of MIL-101(Fe) was successful.

3.4. Mechanism exploration

As shown in Fig. 4(A), the maximum emission wavelength in the MIL-101(Fe)-luminol system is 450 nm, which is the same as the luminol system. This means that the excited 3-aminophthalate anion in the MIL-101(Fe)-luminol system is the luminophore. H_2O_2 is decomposed into free radicals by MIL-101 (Fe) to undergo a chemiluminescence reaction with luminol. Phenylhydrazine and thiourea are $\cdot O_2^-$ and $\cdot OH$ radical quenchers, respectively. As shown in Fig. 4(B), phenylhydrazine and thiourea were added to the system to prove the existence of $\cdot O_2^-$ and $\cdot OH$ radicals. It was also found that the chemiluminescence intensity of the system containing the catalyst MIL-101 (Fe) was more than 5 times that of the system without MIL-101 (Fe). Next, experiments were performed in

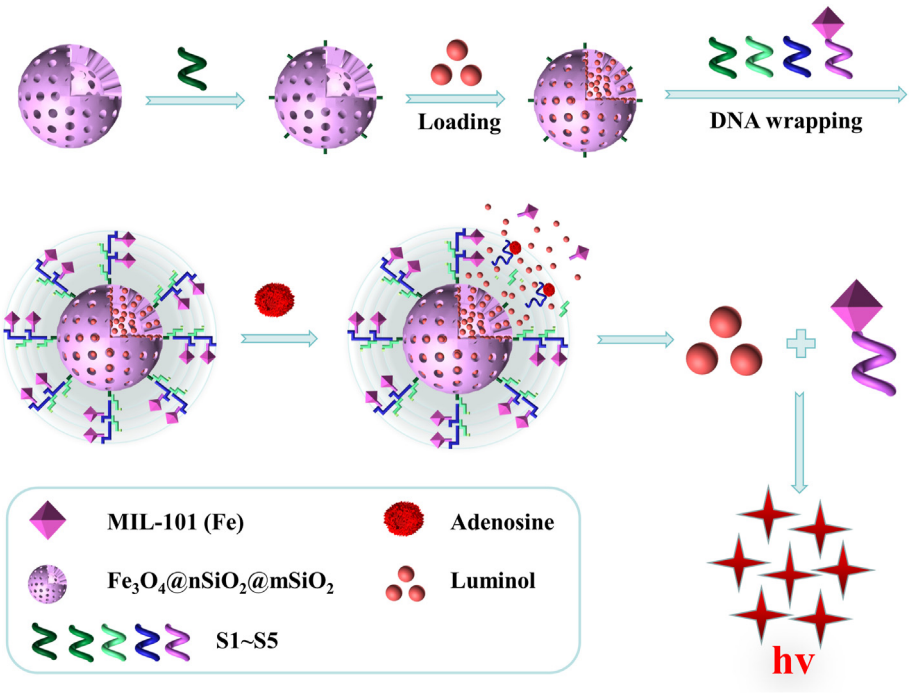

Fig. 1. Schematic illustration of the CL biosensor.

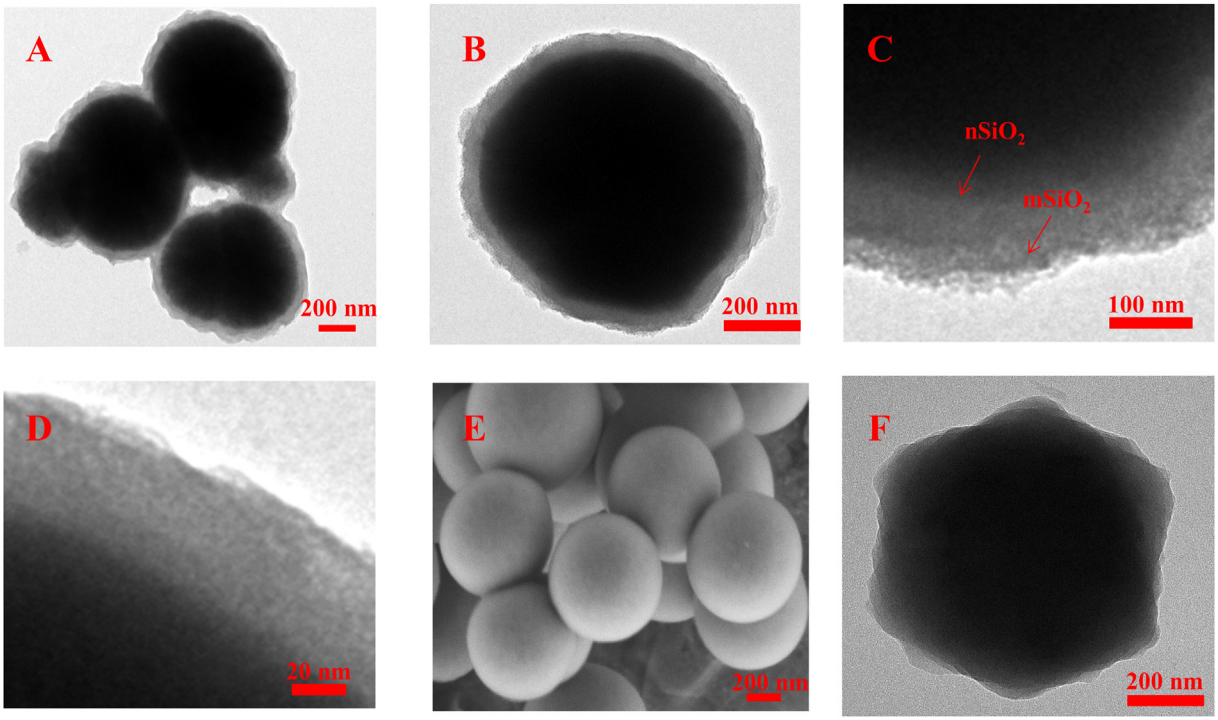

Fig. 2. The TEM images (A–D) and SEM image (E) of Fe_3O_4@nSiO_2@mSiO_2, the TEM imageof Fe_3O_4@nSiO_2@mSiO_2-MIL-101(Fe) (F).

N_2, O_2 and air atmospheres, and it was found that oxygen is of vital importance in chemiluminescence biosensors.

3.5. Optimization of experimental conditions

A standard curve of luminol was drawn with the concentration range of 0.4–4.0 mol/L 50 μL 0.1 mg/μL Fe_3O_4@nSiO_2@mSiO_2-S1, 1.2 mL 0.01 M luminol and 50 μL 10^{-5} M S2 into a 50 mL volumetric flask. And shake for 24 h at 37 °C to detect the CL signal of the supernatant. Calculate the loading of Fe_3O_4@nSiO_2@mSiO_2. In Fig. 5(A), the chemiluminescence value of the supernatant after Fe_3O_4@nSiO_2@mSiO_2 was loaded with luminol. According to the calculation, the saturation capacity of luminol on Fe_3O_4@nSiO_2@mSiO_2 was $Q = n_{luminol}$:nFe_3O_4@nSiO_2@mSiO_2 = 1.12 μmol/mg (194.42 μg/mg),

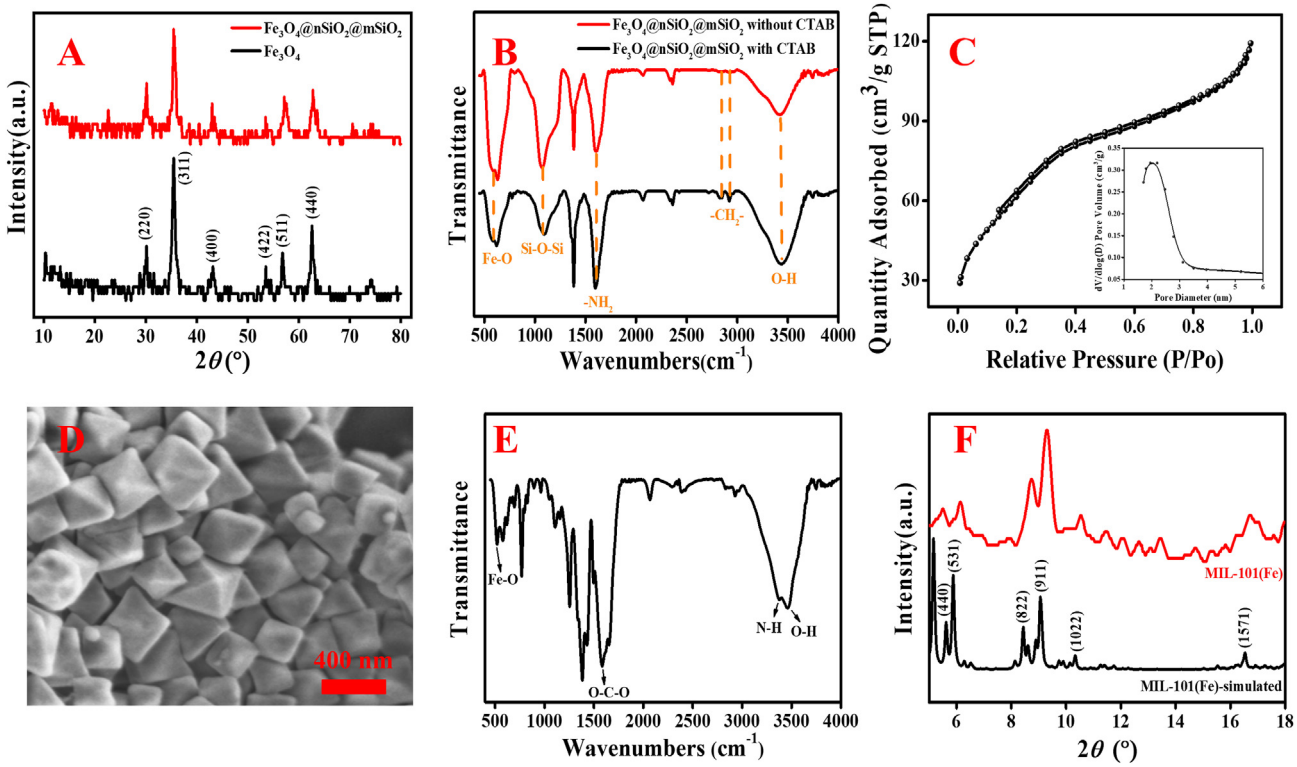

Fig. 3. The XRD pattern (A), FTIR spectra (B) and BET (C) of Fe_3O_4@nSiO_2@mSiO_2; The SEM images (D), FTIR spectra (E) and XRD pattern (F) of MIL-101(Fe).

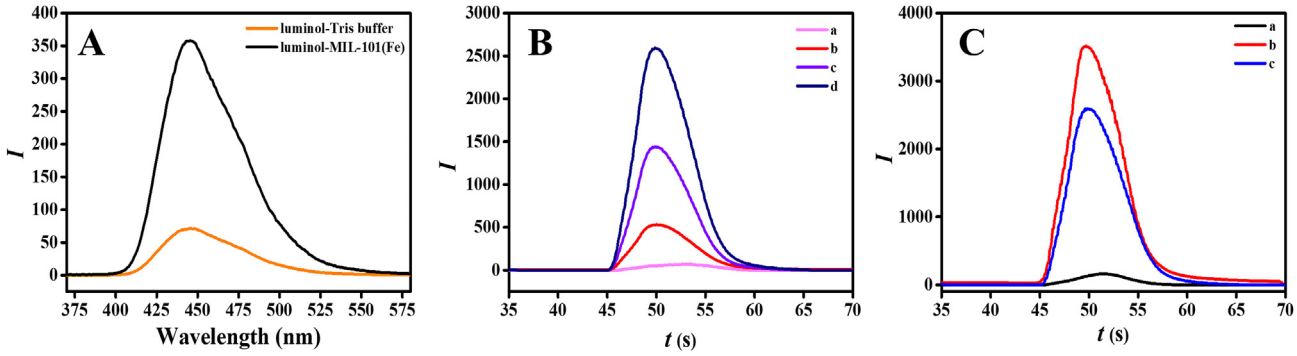

Fig. 4. The CL spectrum. (A) luminol-H_2O_2 and luminol-MIL-101 (Fe)–H_2O_2. (B) luminol -MIL-101 (Fe)–H_2O_2-phenylhydrazine (a); luminol -PBS-H_2O_2 (b); luminol -MIL-101 (Fe)–H_2O_2-thiourea (c); luminol -MIL-101 (Fe)–H_2O_2 (d). (C) luminol -MIL-101 (Fe)–H_2O_2–N_2 (a); luminol -MIL-101 (Fe)–H_2O_2–O_2 (b); luminol -MIL-101 (Fe)–H_2O_2-air(c). luminol: 3.0×10^{-4} mol/L; MIL-101 (Fe): 0.02 mg/mL; NaOH: 0.05 mol/L; H_2O_2: 0.04 mol/L.

which means 198.42 μg of luminol is loaded on 1 mg of Fe_3O_4@n-SiO_2@mSiO_2. A series of 50 μL 0.1 mg/μL Fe_3O_4@nSiO_2@mSiO_2-S1, 560 μL 0.01 M luminol and 50 μL 10^{-5} M S2 were prepared. The above solutions were adjusted to 50 mL with Tris buffer. Pipette the mixed solution of different loading time, detect the chemiluminescence signal and compare the intensity with the chemiluminescence analyzer. According to the change of chemiluminescence intensity, the optimal loading time of Fe_3O_4@nSiO_2@mSiO_2 to luminol was measured. Fig. 5(B) showed the study of the optimal loading time of Fe_3O_4@nSiO_2@mSiO_2 loading luminol. The CL intensity decreases with the increase of loading time, which is caused by the gradual loading of luminol into Fe_3O_4@nSiO_2@mSiO_2. After 3 h, the chemiluminescence signal was stable, indicating that the loading reaction was complete. Therefore, the loading time was 3 h. Fig. 5(B) also further proved that the adsorption capacity of Fe_3O_4@nSiO_2@mSiO_2 loaded luminol was 1.12 μmol/mg.

In this work, luminol-H_2O_2 was used as the chemiluminescence system. In order to obtain the maximum chemiluminescence intensity to ensure the system has high sensitivity, the luminescence conditions that can affect the chemiluminescence intensity of the system were optimized by controlling the single variable method. As shown in Fig. 5 (C—F), the optimal conditions for the flow rate of the main pump, the flow rate of the vice pump, the concentration of NaOH and the concentration of H_2O_2 were 15 r/min, 35 r/min, 0.050 mol/L and 0.04 mol/L, respectively. Furthermore, optimize the reaction time of adenosine and hydrogel shell. Adenosine stimulates the hydrogel shell, Fe_3O_4@nSiO_2@mSiO_2 releases luminol to produce chemiluminescence signals. In the absence of adenosine, the possibility of leakage of Fe_3O_4@nSiO_2@mSiO_2 encapsulated by hydrogel is small. As shown in Fig. 6(A), the optimal time for adenosine to react with the hydrogel shell was 60 min.

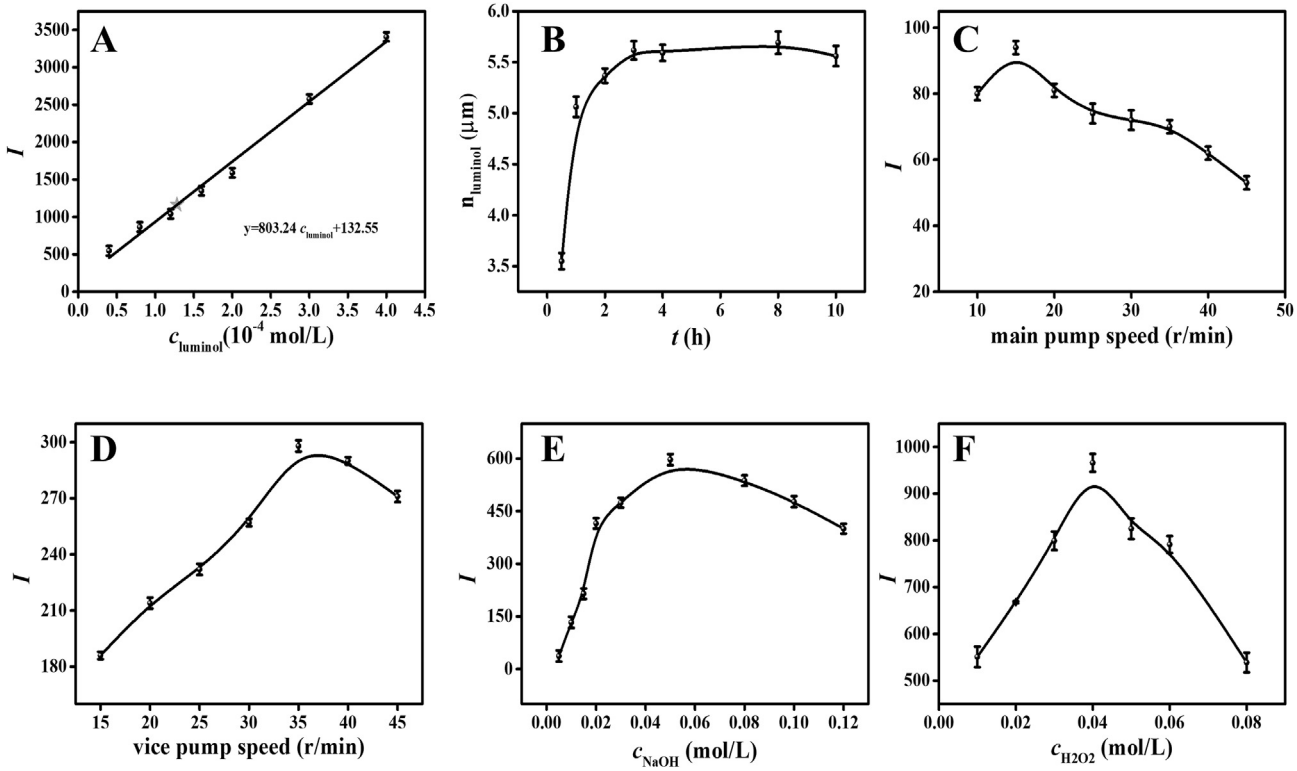

Fig. 5. Study on loading amount (A) and loading time (B) of luminol loaded with Fe_3O_4@nSiO_2@mSiO_2. The optimization of main pump speed (C) and vice pump speed (D). The concentrations optimization of NaOH (E) and H_2O_2 (F). All CL experiments were performed with Tris buffer solution at pH 7.4.

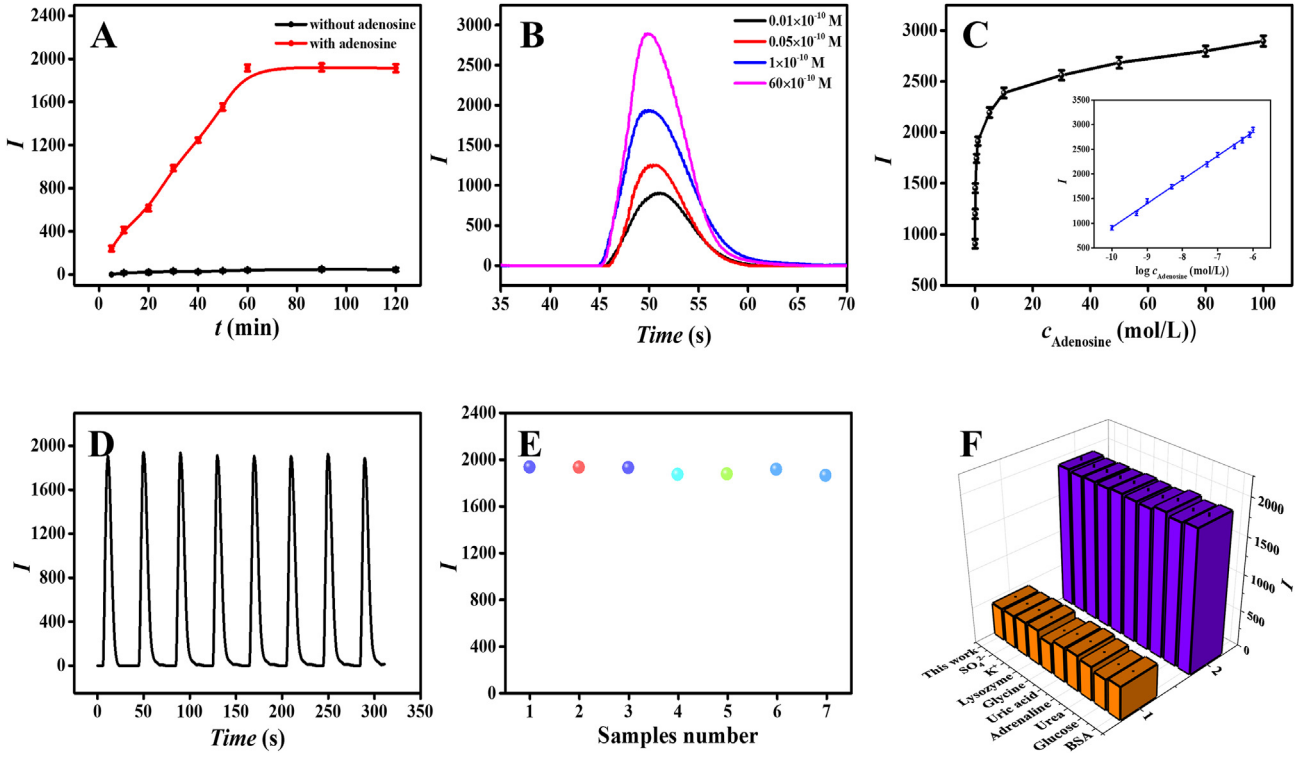

Fig. 6. Optimization of the reaction time between adenosine and hydrogel (A). Study on chemiluminescence signals by different concentration of adenosine (B). The regression equation (C), reproducibility (D, E), selectivity (F) study of the CL biosensor. 0.04 mol/L H_2O_2, 0.05 mol/L NaOH, 0.5 × 10^{-8} mol/L adenosine, 0.5 × 10^{-8} mol/L lysozyme, 0.5 × 10^{-8} mol/L glycine, 0.5 × 10^{-8} mol/L uric acid, 0.5 × 10^{-8} mol/L epinephrine, 0.5 × 10^{-8} mol/L urea, 0.5 × 10^{-8} mol/L glucose, 0.5 × 10^{-8} mol/L BSA, 0.001 mol/L SO_4^{2-} and 0.001 mol/L K^+. CL experiments were performed with Tris buffer solution at pH 7.4. Error bars of all graphs (n = 3).

Table 1
Comparison results of different methods.

Methods	Liner range (mol/L)	Detection limit (mol/L)	references
colorimetric biosensor	2×10^{-6} - 50×10^{-6}	1.7×10^{-6}	[48]
colorimetric biosensor	5×10^{-6} - 50×10^{-6}	0.48×10^{-6}	[49]
electrochemical biosensor	10×10^{-9} - 100×10^{-9}	10×10^{-9}	[50]
SERS biosensor	5×10^{-9} - 5×10^{-7}	5×10^{-9}	[51]
ECL biosensor	1.0×10^{-9} - 1.0×10^{-8}	2.7×10^{-10}	[52]
electrochemical biosensor	5×10^{-9} - 2000×10^{-9}	5×10^{-9}	[53]
fluorescence biosensor	1×10^{-6} - 6×10^{-5}	1.3×10^{-7}	[54]
This work	0.01×10^{-8} - 100×10^{-8}	1.4×10^{-10}	–

3.6. Analytical performances study

In Fig. 6(B), the chemiluminescence signal increases with the increase of adenosine concentration in the solution, which lays the foundation for the subsequent detection of adenosine. Based on the above exploration, a series of standard concentration adenosine solutions were prepared. Under the best experimental conditions, the flow rate of the main pump was 15 r/min, the flow rate of the vice pump was 35 r/min, the NaOH concentration was 0.050 mol/L, and the concentration of H_2O_2 was 0.04 mol/L, the chemiluminescence intensity of adenosine solution was measured. The drawn working curve was shown in Fig. 6(C). In the range of adenosine concentration of 0.01×10^{-8} mol/L-100×10^{-8} mol/L, there was a good linear correlation between chemiluminescence intensity and logarithm of adenosine concentration, the linear equation was $I = 5762.27 + 484.74 \log c_{adenosine}$, $R^2 = 0.99$, the detection limit was 1.4×10^{-10} mol/L. The chemiluminescence intensity increased with the increase of adenosine concentration in the system. Because as the concentration of adenosine increases, the hydrogel shell was hydrolyzed, the luminol was released from Fe_3O_4@nSiO_2@mSiO_2, and MIL-101 (Fe) catalyst enters the solution, which leads to the enhancement of chemiluminescence signal.

Table 1 showed the comparison between this work and platforms that have been published to detect adenosine. Among the many distinguished detection platforms, the chemiluminescence method still has the advantage of high sensitivity.

3.7. Repeatability and selectivity performances study

The reproducibility study of the sensing platform was shown in Fig. 6 (D, E). Fig. 6 (D) shown that continuous detection of the chemiluminescence signal of the same sample, and it is found that the change of the chemiluminescence signal was within a controllable range. Moreover, seven samples of the same concentration were prepared to study the difference between duplicate samples. As shown in Fig. 6(E), the RSD of the chemiluminescence signal in the seven samples was 2.0%. In this work, the sample with only adenosine standard solution was the control group. The chemiluminescence signals were detected on the solutions containing interfering substances such as lysozyme, glycine, uric acid, epinephrine, urea, glucose, bovine serum albumin (BSA), SO_4^{2-} and K^+. All the selected interferers are easily existing or common substances in the body environment. In addition, interference experiments were also carried out on the chemiluminescence method for detecting adenosine in the absence of MIL-101 (Fe). Fig. 6(F) shows that the relative error of the intensity signals of this proposed method was 1.5% while that of the simple chemiluminescence method was 6.4%. This proves that the proposed chemiluminescence aptamer sensor has good selectivity and anti-interference ability.

3.8. Application of the CL biosensor

As shown in Table S1, under the best experimental conditions, this method was used to detect the adenosine content in urine. The recovery rate of standard addition was between 98.0% and 102.6%. These results indicate that this method can productively analyze adenosine in actual samples.

4. Conclusions

All in all, the constructed biosensor based on DNA cross-linked hydrogel-capped magnetic core-shell structure mesoporous silica nanoparticles has the following advantages: (1) Through DNA cross-linked hydrogel-capped mesoporous silica nanoparticles, the loading rate of Fe_3O_4@nSiO_2@mSiO_2 was effectively increased. (2) The aptamer DNA chain acts as a "switch" to prevent luminol from leaking in advance. (3) The aptamer DNA chain specifically recognizes adenosine, and the released luminol as the signal molecule in the luminol chemiluminescence system. (4) The peroxidase-like MIL-101 (Fe) loaded by DNA hydrogel has the effect of amplifying the signal. In addition, the biosensor has been successfully applied to the detection of adenosine in actual samples. This work can provide theoretical help for other detection methods to detect tumor markers. However, the proposed biosensor is currently only available to detect adenosine in urine at the laboratory level, and more samples need to be tested. Therefore, further research is needed before the biosensor can be used in medicine.

CRediT authorship contribution statement

Yanan Hou: Conceptualization, Formal analysis, Data curation, Methodology, Writing – original draft. **Rui Han:** Visualization, Investigation. **Yuanling Sun:** Investigation, Visualization. **Chuannan Luo:** Conceptualization, Writing – review & editing, Validation. **Xueying Wang:** Supervision, Validation.

Declaration of competing interest

We declare that we have no financial and personal relationships with other people or organizations that can inappropriately influence our work, there is no professional or other personal interest of any nature or kind in any product, service and/or company that could be construed as influencing the position presented in, or the review of, the manuscript entitled, "Chemiluminescence sensing of adenosine using DNA cross-linked hydrogel-capped magnetic mesoporous silica nanoparticles".

Acknowledgments

This work was supported by the Shandong Provincial Natural Science Foundation of China (No. ZR2016BM01), Horizontal

Scientific Research Project of China (No. W15077), National Natural Science Foundation of China (No. 21605094), and Shandong Province Natural Science Institute Joint Fund (No. ZR2015YL006).

The authors would like to thank Li Yankai from Shiyanjia Lab (www.shiyanjia.com) for the TEM analysis.

Appendix A. Supplementary data

Supplementary data to this article can be found online at https://doi.org/10.1016/j.aca.2021.339386.

References

[1] M. Mujoomdar, D. Hoskin, J. Blay, Adenosine stimulation of the proliferation of colorectal carcinoma cell lines: roles of cell density and adenosine metabolism [J], Biochem. Pharmacol. 66 (9) (2003) 1737–1747.
[2] Y. Lin, X. Wang, Y. Sun, et al., A chemiluminescent biosensor for ultrasensitive detection of adenosine based on target-responsive DNA hydrogel with Au@HKUST-1 encapsulation[J], Sensor. Actuator. B Chem. 289 (2019) 56–64.
[3] P.P. Chaudhari, L.K. Chau, Y.T. Tseng, et al., A fiber optic nanoplasmonic biosensor for the sensitive detection of ampicillin and its analogs[J], Mikrochim. Acta 187 (7) (2020) 396.
[4] M. Qing, S.L. Chen, L. Han, et al., Three-dimensional donor-acceptor-type photoactive material/conducting polyaniline hydrogel complex for sensitive photocathodic enzymatic bioanalysis[J], Biosens. Bioelectron. 158 (2020) 112179.
[5] E. Stavra, P.S. Petrou, G. Koukouvinos, et al., Fast, sensitive and selective determination of herbicide glyphosate in water samples with a White Light Reflectance Spectroscopy immunosensor[J], Talanta 214 (2020) 120854.
[6] J. Jeon, J. Lee, J.-I. So, et al., Homogeneous fluorescent aptasensor for active tuberculosis diagnosis by direct quantification of circulating TB7.7 based on aptamer beacon with graphene oxide[J], Sensor. Actuator. B Chem. (2020) 317.
[7] C. Hong, R. Cai, W. Tan, et al., Aptamer-pendant DNA tetrahedron nanostructure probe for ultrasensitive detection of tetracycline by coupling target-triggered rolling circle amplification[J], ACS Appl. Mater. Interfaces 17 (2021) 19695–19700.
[8] J. Ge, D. Yang, R. Cai, W. Tan, et al., Highly sensitive MicroRNA detection by coupling nicking-enhanced rolling circle amplification with MoS_2 quantum dots[J], Anal. Chem. 92 (2020) 13588–13594.
[9] N. Xiao, R. Wu, J.J. Huang, et al., Anode surface modification regulates biofilm community population and the performance of micro-MFC based biochemical oxygen demand sensor[J], Chem. Eng. Sci. (2020) 221.
[10] S. Dai, Y. Zhou, G. Cheng, et al., Dual-signal electrochemical sensor for detection of cancer cells by the split primer ligation-triggered catalyzed hairpin assembly[J], Talanta 217 (2020) 121079.
[11] J. Ge, R. Cai, et al., Human serum albumin templated MnO_2 nanosheets as an efficient biomimetic oxidasefor biomolecule sensing[J], J. Mater. Chem. B 8 (2020) 11090–11095.
[12] C. Hong, H. Yang, D. Yang, R. Cai, W. Tan, et al., On-Site colorimetric detection of cholesterol based on polypyrrole nanoparticles[J], ACS Appl. Mater. Interfaces 12 (2020) 54426–54432.
[13] C. Hong, Z. Huang, R. Cai, W. Tan, et al., Green Synthesis of Au@WSe_2 Hybrid Nanostructures with the Enhanced Peroxidase-like Activity for Sensitive Colorimetric Detection of glucose[J], Nano Research, 2021, https://doi.org/10.1007/s12274-021-3706-3.
[14] R. Cai, L. Yan, Y. Zhao, W. Tan, et al., Plasmonic AuPt@CuS heterostructure with enhanced synergistic efficacy for radiophotothermal therapy[J], J. Am. Chem. Soc. 143 (2021) 16113–16127.
[15] M. Kong, P. Jin, W. Wei, et al., Covalent organic frameworks (COF-300-AR) with unique catalytic performance in luminol chemiluminescence for sensitive detection of serotonin[J], Microchem. J. (2021) 160.
[16] C.-L. Shen, Q. Lou, K.-K. Liu, et al., Chemiluminescent carbon dots: synthesis, properties, and applications[J], Nano Today (2020) 35.
[17] L. Montali, M.M. Calabretta, A. Lopreside, et al., Multienzyme chemiluminescent foldable biosensor for on-site detection of acetylcholinesterase inhibitors [J], Biosens. Bioelectron. 162 (2020) 112232.
[18] L. He, Z.W. Jiang, W. Li, et al., In situ synthesis of gold nanoparticles/metal-organic gels hybrids with excellent peroxidase-like activity for sensitive chemiluminescence detection of organophosphorus pesticides[J], ACS Appl. Mater. Interfaces 10 (34) (2018) 28868–28876.
[19] Y. Lu, X. Zhang, X. Mao, et al., Engineering FeCo alloy@N-doped carbon layers by directly pyrolyzing Prussian blue analogue: new peroxidase mimetic for chemiluminescence glucose biosensing[J], J. Mater. Chem. B 7 (30) (2019) 4661–4668.
[20] Z. Song, J. Lü, T. Zhao, Chemiluminescence sensor for isoniazid with controlled-reagent-release technology[J], Talanta 53 (2001) 1171–1177.
[21] Z. Song, N. Zhang, In vitro monitoring sub-nanogram amounts analgin in human urine by its inhibitory of the luminol-periodate chemiluminescence reaction using reagent immobilization release technique[J], Bioorg. Med. Chem. 10 (2002) 2091–2097.
[22] P. Huang, X. Zeng, et al., New Advances in Gated Materials of Mesoporous Silica for Drug Controlled release[J], Chinese Chemical Letters, 2021.
[23] Y. Kong, X. Li, X. Liu, J. Pang, et al., Galactosylated chitosan modified magnetic mesoporous silica nanoparticles loaded with nedaplatin for the targeted chemo-photothermal synergistic therapy of cancer[J], J. Nanosci. Nanotechnol. 21 (2021) 4553–4564.
[24] W. Si, Y. Gao, X. Mei, et al., Mesoporous silica nanoparticles loaded with capsaicin and their oxidation resistance in meat preservation[J], Food Chem. 344 (2021) 128737.
[25] C. Guo, Y. Zhang, Y. Li, et al., Gold nanoparticle-guarded large-pore mesoporous silica nanocomposites for delivery and controlled release of cytochrome c[J], J. Colloid Interface Sci. 589 (2021) 34–44.
[26] T.-H. Lo, Z.-Y. Wu, S.-Y. Chen, et al., Curcumin-loaded mesoporous silica nanoparticles with dual-imaging and temperature control inhibits the infection of Zika virus[J], Microporous Mesoporous Mater. (2021) 314.
[27] N. Zhang, C. Jia, X. Ma, et al., Hierarchical core-shell Fe_3O_4@mSiO_2@Chitosan nanoparticles for pH-responsive drug delivery[J], J. Nanosci. Nanotechnol. 21 (2021) 3020–3027.
[28] M. Oroval, C. Coll, A. Bernardos, et al., Selective fluorogenic sensing of as(III) using aptamer-capped nanomaterials[J], ACS Appl. Mater. Interfaces 9 (13) (2017) 11332–11336.
[29] Z. Gu, A. Fu, L. Ye, et al., Ultrasensitive chemiluminescence biosensor for nuclease and bacterial determination based on hemin-encapsulated mesoporous silica nanoparticles[J], ACS Sens. 4 (11) (2019) 2922–2929.
[30] Q. Zhang, X. Liu, L. Duan, et al., A DNA-inspired hydrogel mechanoreceptor with skin-like mechanical behavior[J], J. Mater. Chem. 9 (3) (2021) 1835–1844.
[31] H.S. Kim, N. Abbas, S. Shin, A rapid diagnosis of SARS-CoV-2 using DNA hydrogel formation on microfluidic pores[J], Biosens. Bioelectron. 177 (2021) 113005.
[32] F. Mo, K. Jiang, D. Zhao, et al., DNA hydrogel-based gene editing and drug delivery systems[J], Adv. Drug Deliv. Rev. 168 (2021) 79–98.
[33] S. Okumura, B.N. Hapsianto, N. Lobato-Dauzier, et al., Morphological manipulation of DNA gel microbeads with biomolecular stimuli, J. Nanomater. 11 (2) (2021) 293.
[34] J. Yao, Yue, C. Huang, H. Wang, A magnified aptamer fluorescence sensor based on the metal organic frameworks adsorbed DNA with enzyme catalysis amplification for ultra-sensitive determination of ATP and its logic gate operation[J], Bioorg. Chem. 114 (2021) 105020.
[35] R. Han, Y. Sun, Y. Dai, D. Gao, X. Wang, C. Luo, A chemiluminescence aptasensor for sensitive detection of carcinoembryonic antigen based on dual aptamer-conjugates biorecognition[J], Sensor. Actuator. B Chem. 326 (2021) 128833.
[36] H. Wang, W. Fu, Y. Chen, F. Xue, G. Shan, ZIF-67-derived Co_3O_4 hollow nanocage with efficient peroxidase mimicking characteristic for sensitive colorimetric biosensing of dopamine[J], Spectrochim. Acta Mol. Biomol. Spectrosc. 246 (2021) 119006.
[37] S. Yue, S. Bi, et al., An enzyme-free molecular catalytic device: dynamically self-assembled DNA dendrimers for in situ imaging of microRNAs in live cells [J], Chem. Sci. 10 (2019) 1651–1658.
[38] K. Yu, X. Hai, S. Yue, W. Song, S. Bi, Glutathione-activated DNA-Au nanomachine as targeted drug delivery platform for imaging-guided combinational cancer therapy[J], Chem. Eng. J. 419 (2021) 129535.
[39] K. Yu, S. Bi, et al., DNA nanotechnology for multimodal synergistic theranostics[J], Journal of Analysis and Testing 5 (2021) 112–129.
[40] S. Yue, Y. Li, Z. Qiao, W. Song, S. Bi, Rolling circle replication for biosensing, bioimaging, and biomedicine[J], Trends Biotechnol. 39 (2021) 1160–1172.
[41] Y. Song, L. He, S. Zhang, et al., Novel impedimetric sensing strategy for detecting ochratoxin A based on NH_2-MIL-101(Fe) metal-organic framework doped with cobalt phthalocyanine nanoparticles[J], Food Chem. 351 (2021) 129248.
[42] D. Hou, Y. You, X. Wu, et al., A nanosized metal–organic framework for visual detection of fluoride ions with smartphone via colorimetric test kit[J], Sensor. Actuator. B Chem. (2021) 332.
[43] S. Yuan, X. Bo, L. Guo, In-situ insertion of multi-walled carbon nanotubes in the Fe3O4/N/C composite derived from iron-based metal-organic frameworks as a catalyst for effective sensing acetaminophen and metronidazole[J], Talanta 193 (2019) 100–109.
[44] J. He, G. Li, Y. Hu, Aptamer-involved fluorescence amplification strategy facilitated by directional enzymatic hydrolysis for bioassays based on a metal-organic framework platform: highly selective and sensitive determination of thrombin and oxytetracycline[J], Microchim. Acta 184 (7) (2017) 2365–2373.
[45] Q. Luan, X. Xiong, N. Gan, et al., A multiple signal amplified colorimetric aptasensor for antibiotics measurement using DNAzyme labeled Fe-MIL-88-Pt as novel peroxidase mimic tags and CSDP target-triggered cycles[J], Talanta 187 (2018) 27–34.
[46] Y. Deng, D. Qi, C. Deng, et al., Superparamagnetic high-magnetization microspheres with an Fe $_3O_4$@SiO_2 core and perpendicularly aligned mesoporous SiO_2 shell for removal of microcystins[J], J. Am. Chem. Soc. 130 (2008) 28–29.
[47] D. Wang, F. Jia, H. Wang, et al., Simultaneously efficient adsorption and photocatalytic degradation of tetracycline by Fe-based MOFs[J], J. Colloid Interface Sci. 519 (2018) 273–284.
[48] Y. Tao, F. Luo, L. Guo, et al., Target-triggered aggregation of gold nanoparticles for photothermal quantitative detection of adenosine using a thermometer as readout[J], Anal. Chim. Acta 1110 (2020) 151–157.

[49] S. Zhou, Y. Gan, L. Kong, et al., A novel portable biosensor based on aptamer functionalized gold nanoparticles for adenosine detection[J], Anal. Chim. Acta 1120 (2020) 43–49.
[50] F. Yan, F. Wang, Z. Chen, Aptamer-based electrochemical biosensor for label-free voltammetric detection of thrombin and adenosine[J], Sensor. Actuator. B Chem. 160 (1) (2011) 1380–1385.
[51] S. Xu, B. Man, S. Jiang, et al., Graphene/Cu nanoparticle hybrids fabricated by chemical vapor deposition as surface-enhanced Raman scattering substrate for label-free detection of adenosine[J], ACS Appl. Mater. Interfaces 7 (2015) 10977–10987.
[52] S. Ye, H. Li, W. Cao, Electrogenerated chemiluminescence detection of adenosine based on triplex DNA biosensor[J], Biosens. Bioelectron. 26 (5) (2011) 2215–2220.
[53] C. Sun, X. Liu, K. Feng, et al., An aptazyme-based electrochemical biosensor for the detection of adenosine[J], Anal. Chim. Acta 669 (2010) 87–93.
[54] W. Li, J. Sun, H. Wang, et al., Multifunctional aptamer probe mediated cascade amplification for label-free detection of adenosine[J], Sensor. Actuator. B Chem. 260 (2018) 581–586.